ACS Catalysis

Research Article

pubs.acs.org/acscatalysis

Mechanism and Catalytic Impact of Ir−Ta Heterobimetallic and Ir−P Transition Metal/Main Group Interactions on Alkene Hydrogenation

Ying Zhang,[‡] Samuel P. Roberts,[‡] Robert G. Bergman,[†] and Daniel H. Ess*[,‡]

[‡]Department of Chemistry and Biochemistry, Brigham Young University, Provo, Utah 84602, United States

[†]Department of Chemistry, University of California, Berkeley, California 94720, United States

Supporting Information

ABSTRACT: Transition metal heterobimetallic catalysts provide an alternative to classic transition metal ligand catalyst design. The resurgence in popularity of heterobimetallic complexes prompted our use of density functional theory to examine the mechanism and reactivity of alkene hydrogenation catalyzed by the transition metal heterobimetallic complex $Cp_2Ta(CH_2)_2Ir(CO)(PPh_3)$ and the transition metal/main group complex $Ph_2P(CH_2)_2Ir(CO)(PPh_3)$. Calculations indicate that the Ir−Ta and Ir−P catalysts operate by different mechanisms. For the Ir−Ta complex, initial H_2 oxidative addition to the Ir metal center followed by reductive elimination of an Ir−H and μ-CH_2 bridge transforms the starting heterobimetallic complex into an active Ir−H catalyst. This catalyst precursor transformation occurs because the cationic Cp_2Ta group provides a low activation barrier for reductive elimination. This transformation does not occur for the Ir−P catalyst because the reductive elimination activation barrier is significantly higher in energy. The active heterobimetallic Ir−H likely catalyzes multiple turnovers of alkene hydrogenation before reforming the original heterobimetallic Ir−Ta complex. The Ir−H catalytic cycle involves a series of classic organometallic reaction steps: alkene migratory insertion, H_2 oxidative addition, and reductive elimination. In the Ir−P mechanism, the $Ph_2P(CH_2)_2$ group remains as a spectator ligand throughout the active catalytic cycle. The Ir−P catalytic cycle involves H_2 oxidative addition, phosphine ligand dissociation, ethylene migratory insertion, and reductive elimination.

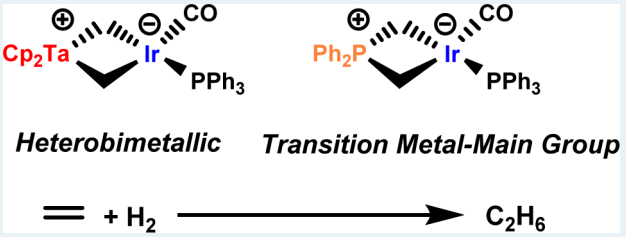

KEYWORDS: *heterobimetallic, density functional theory, catalysis, alkene hydrogenation, mechanism, iridium, tantalum*

INTRODUCTION

Transition metal heterobimetallic complexes with a direct metal−metal interaction provide a unique platform for chemical reactivity due to the potential for cooperative effects between metal centers.[1,2] For example, a heterobimetallic metal−metal interaction may facilitate an oxidation state change, enhance electrophilicity/nucleophilicity, or completely alter a reaction mechanism. Heterobimetallic complexes[3] provide an alternative to the classic ligand-to-single-metal structure of mononuclear complexes and are generally designed so that either both metals are involved in bond formation events or the second metal acts as an active ligand support.

In the past few years, there has been a resurgence in the synthesis,[4−7] structural and electronic characterization,[8−10] and application of heterobimetallic complexes.[11−14] Catalytic early late heterobimetallic complexes have been reported for cross-coupling,[15] allyl amination,[16] hydrosilylation,[17] hydroformylation,[18] ethylene polymerization,[19] alkyne cyclotrimerization,[20] and CH borylation.[21]

Our group is involved in using density functional theory (DFT) to understand mechanisms and origins of enhanced catalytic reactivity for heterobimetallic complexes compared with monometallic complexes. Here, we report DFT modeling of alkene hydrogenation catalyzed by the heterobimetallic transition metal complex $Cp_2Ta(CH_2)_2Ir(CO)(PPh_3)$ (**1a**) and the transition metal/main group complex $Ph_2P(CH_2)_2Ir(CO)(PPh_3)$ (**1b**) (Scheme 1).[22,23] Calculations reveal, in accord with experiment, that the heterobimetallic Ir−Ta interaction induces a catalytic mechanism that is different from the transition metal/main group Ir−P interaction. Outlined in the Results and Discussion section, our calculations suggest that the heterobimetallic Ir−Ta complex undergoes a precursor transformation in which the starting **1a** complex is converted to an active Ir−H catalyst. The Ir−H species catalyzes multiple

Scheme 1. Ir−Ta and Ir−P Catalysts Reported by Bergman for Alkene Hydrogenation[22]

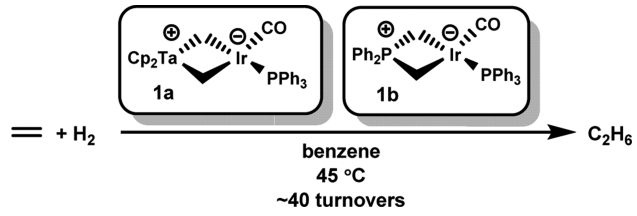

Received: November 26, 2014
Revised: January 30, 2015
Published: February 20, 2015

DOI: 10.1021/cs501884j
ACS Catal. 2015, 5, 1840−1849

Scheme 2. General Alkene Hydrogenation Catalytic Cycles for Complex 1a

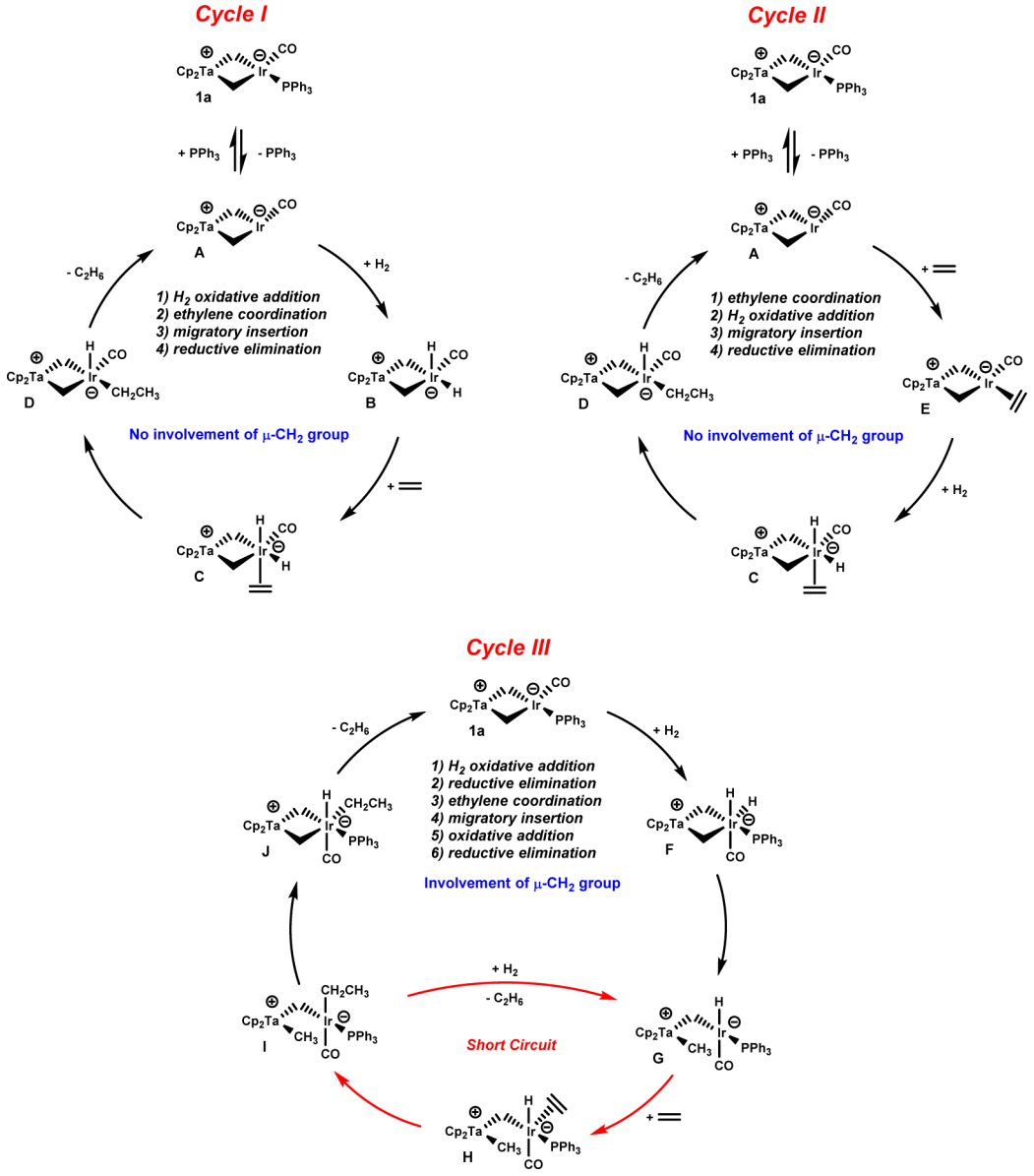

turnovers of alkene hydrogenation via a series of classic organometallic reaction steps before reforming the original Ir−Ta complex. This precursor transformation is not energetically accessible for the Ir−P catalyst, and therefore, a different alkene hydrogenation mechanism operates.

RESULTS AND DISCUSSION

Possible Catalytic Mechanisms. There are several possible mechanisms for alkene hydrogenation by Ir catalysts.[24] Scheme 2 outlines three mechanistic permutations for catalyst **1a**. Catalytic cycle I begins with PPh_3 dissociation to give the 3-coordinate Ir intermediate **A** $[Cp_2Ta(CH_2)_2Ir(CO)]$. Subsequent H_2 coordination and oxidative addition transforms **A** into the 5-coordinate cis dihydride **B** $[Cp_2Ta(CH_2)_2Ir(H)_2(CO)]$. Ethylene coordination gives the octahedral intermediate **C** that then undergoes migratory insertion to give the 5-coordinate Ir−H **D** $[Cp_2Ta(CH_2)_2Ir(H)(CO)(Et)]$. Reductive elimination generates ethane and PPh_3 recoordination returns complex **1a** that is off cycle.

Catalytic cycle II also involves PPh_3 dissociation to give intermediate **A**. This is followed by ethylene coordination to give intermediate **E** $[Cp_2Ta(CH_2)_2Ir(C_2H_4)(CO)]$. Subsequent H_2 oxidative addition and ethylene migratory insertion steps are identical with those of catalytic cycle I. In both cycles I and II, all reaction steps occur at the Ir metal center without the direct involvement of the $Cp_2Ta(CH_2)_2$ ligand scaffold.

Catalytic cycle III involves an important mechanistic twist compared with catalytic cycles I and II. The cycle begins with H_2 oxidative addition to give the 6-coordinate cis dihydride **F** $[Cp_2Ta(CH_2)_2Ir(H)_2(CO)(PPh_3)]$. Rather than PPh_3 dissociation to generate a vacant coordination site for ethylene coordination, reductive elimination of the μ-CH_2 group and hydride results in the formally square planar intermediate **G** $[Cp_2Ta(CH_3)(CH_2)Ir(H)(CO)(PPh_3)]$. Ethylene coordination and migratory insertion steps result in the Ir−H ethyl intermediate **I** $[Cp_2Ta(CH_2)_2Ir(H)(Et)(CO)(PPh_3)]$. At this stage of the catalytic cycle, the $Ta(CH_3)$ group then undergoes oxidative addition to form intermediate **J** $[Cp_2Ta(CH_2)_2Ir(H)$-

DOI: 10.1021/cs501884j
ACS Catal. 2015, 5, 1840−1849

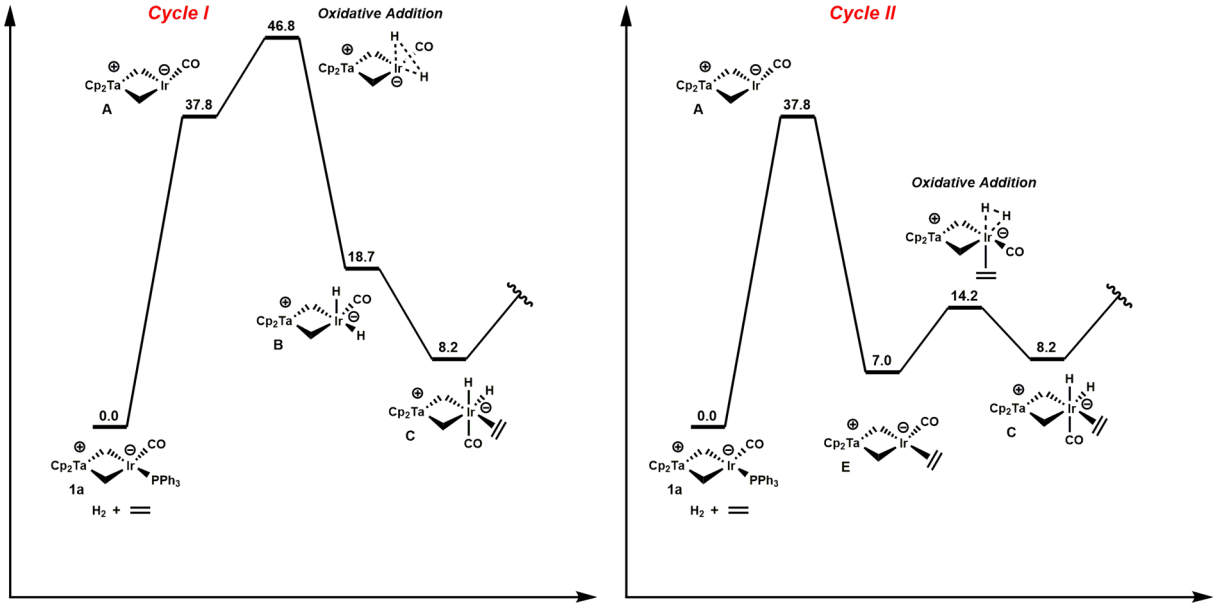

Figure 1. M06 enthalpy landscape for phosphine dissociation, H_2 oxidative addition, and ethylene coordination in catalytic cycles I and II. (kcal/mol).

$(Et)(CO)(PPh_3)$]. Subsequent reductive elimination generates ethane and completes the catalytic cycle to reform complex **1a**.

As an alternative to the full catalytic cycle III, there is a short circuit pathway shown in red where ethane is generated by H_2 addition to the Ir−H intermediate **I**. This reaction step forms intermediate **G** and bypasses reforming the original hetero-bimetallic complex **1a**. In this shortened catalytic cycle, **1a** is a precatalyst and multiple turnovers occur with an Ir−H catalyst before reforming complex **1a**.

Computational Methods. All optimizations were performed in Gaussian 09[25] with the M06[26] density functional and 6-31G(d,p) basis set for and LANL2DZ pseudopotential/basis set for Ir and Ta ($\Delta E_{(small)}$). Geometries presented were confirmed as minima or saddle points by optimization to a stationary point and then full calculation of the Hessian and vibrational analysis. Key transition-state structures were also examined using intrinsic reaction coordinate calculations to verify the connection to proposed intermediates. Extensive conformation searching was performed for all intermediates and transition-state structures. The structures presented are the lowest energy conformations identified. The M06 density functional was chosen because it provides the best expected accuracy for transition metal and main group species. All energy calculations were performed with an ultrafine integration grid. Electronic energies were improved using the 6-311+G(2d,2p) basis set along with the LAN2TZ(f)[27] pseudopotential/basis set for Ir and Ta ($\Delta E_{(large)}$). All optimizations and single point energy evaluations were carried out in the implicit SMD[28] THF solvent model. Enthalpies and free energies are reported at 298 K. Enthalpies reported are the sum of $\Delta E_{(large)} + \Delta G_{solv(small)} + \Delta E_{ZPE(small)} + \Delta H_{(small)} + n$RT. Free energies include $-T\Delta S$ correction.

Catalytic Cycles for Ir−Ta Catalyst. Both catalytic cycles I and II begin with PPh_3 dissociation. The ΔH for PPh_3 dissociation from complex **1a** is 37.8 kcal/mol. On the free energy surface, ΔG for PPh_3 dissociation from complex **1a** is 23.6 kcal/mol. This enthalpy for PPh_3 dissociation coupled with the $\Delta H^{\ddagger}$ of 9.0 kcal/mol for H_2 oxidation addition to intermediate **A** to give **B** results in an overall $\Delta H^{\ddagger}$ = 46.8 kcal/mol for conversion of **1a** and dihydrogen into **B** (Figure 1, left-hand side). Although subsequent ethylene coordination is thermodynamically favorable, the overall large barrier for H_2 oxidative addition rules out catalytic cycle I. Catalytic cycle II with ethylene coordination prior to H_2 oxidative addition is a lower enthalpy process than cycle I; however, catalytic cycle II is higher in enthalpy than catalytic cycle III discussed below.

The enthalpy landscape for catalytic cycle III is graphically depicted at the top of Figure 2. H_2 coordination and oxidative addition at the Ir metal center via **TS1** transforms the square-planar 4-coordinate Ir metal center into the cis dihydride **F**. **TS1** (Figure 3) requires $\Delta H^{\ddagger}$ = 10.1 kcal/mol. The alternative oxidative addition transition state where the CO group is cis to both partial Ir−H bonds is ∼5 kcal/mol higher in enthalpy. The enthalpy of cis dihydride **F** is −6.7 kcal/mol relative to **1a** and free H_2. This exothermic species is in accord with the observed 1:3 equilibrium ratio of **1a**/**F** at 45 °C reported by Bergman and co-workers.[22] On the free energy surface (Figure 2, bottom) the cis dihydride **F** is 2.0 kcal/mol higher in free energy than **1a**. The experimental 1:3 equilibrium of **1a**/**F** indicates that **F** should be ∼0.5 kcal/mol exergonic compared with **1a**. The predicted slightly endergonic cis dihydride **F** on the free energy landscape is likely due to slight overestimation of translational entropy.

From the cis dihydride **F**, reductive elimination via **TS2** places one of the hydride ligands onto the bridging methylene group to give **G** and regenerates a formally 4-coordinate Ir metal center. In **TS2**, reductive elimination of the hydride group occurs in the plane of the μ-CH_2 bridge (Figure 3). The alternative transition state with reductive elimination of the hydride group perpendicular to the μ-CH_2 bridge requires >10 kcal/mol more enthalpy than **TS2**. This pathway is also lower in enthalpy than PPh_3 dissociation to give **B**.

Inspection of structure **G** suggests that although the Ir is 4-coordinate, there remains a significant dative interaction between the Ir metal center and the Cp_2Ta group. In **1a**, the Ir−Ta distance is 2.89 Å and increases only slightly to 3.00 Å in **G**, and therefore, **1a** should still be considered a hetero-bimetallic complex. This Ir−Ta interaction keeps the $Ta(CH_3)$

DOI: 10.1021/cs501884j
ACS Catal. 2015, 5, 1840−1849

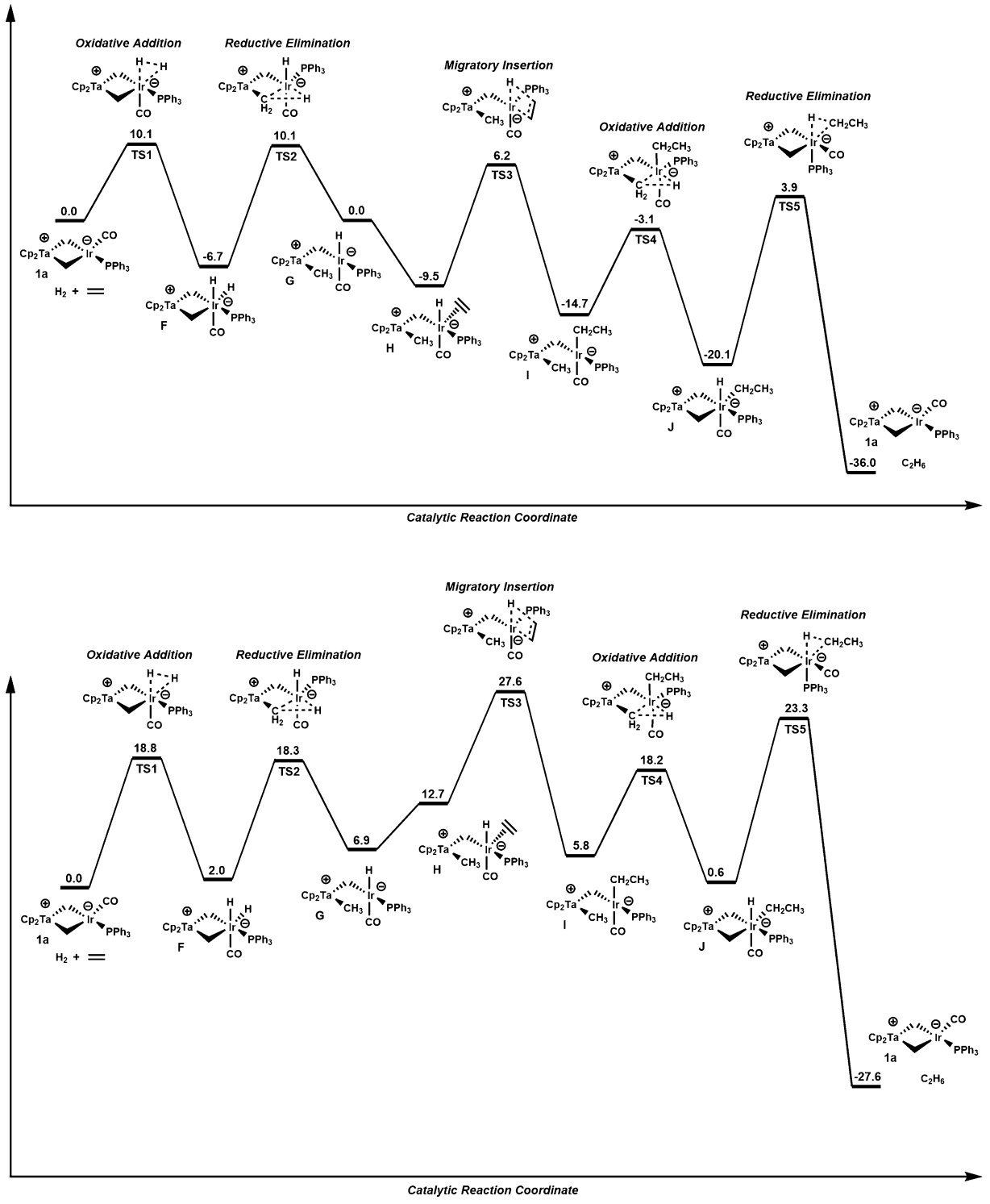

Figure 2. M06 enthalpy (top) and free energy (bottom) landscapes for the complete catalytic cycle III. (kcal/mol).

group in close proximity of the metal center. Rotation about the remaining μ-CH_2 bridge that would partially sever the Ir−Ta interaction is prevented by the bulky Cp groups.

Ethylene coordinates to intermediate **G** in a geometry where it is trans to the weakly interacting Ta-CH_3 group to give **H**. Ethylene coordination is 9.5 kcal/mol exothermic relative to **G**, but on the free energy surface is ∼6 kcal/mol endergonic relative to **G**. The lowest enthalpy transition state for ethylene migratory insertion into the Ir−H bond, **TS3** (Figure 3), requires PPh_3 and ethylene ligand rearrangement. **TS3** requires $\Delta H^{\ddagger}$ = 6.2 kcal/mol and leads to the Ir-Et species **I**. On the free energy surface, **TS3** requires $\Delta G^{\ddagger}$ = 27.6 kcal/mol and this is a higher free energy barrier than H_2 oxidative addition.

Because the Cp_2Ta-CH_3 group remains covalently attached to the Ir metal center via the remaining μ-CH_2 bridge, there is the possibility for oxidative addition via **TS4** to give the iridium hydride. Similar to **TS1** and **TS2**, the $\Delta H^{\ddagger}$ for **TS4** relative to **I** is 11.6 kcal/mol and relative to **1a** is −3.1 kcal/mol. Catalytic cycle III is completed by reductive elimination from iridium

DOI: 10.1021/cs501884j
ACS Catal. 2015, 5, 1840−1849

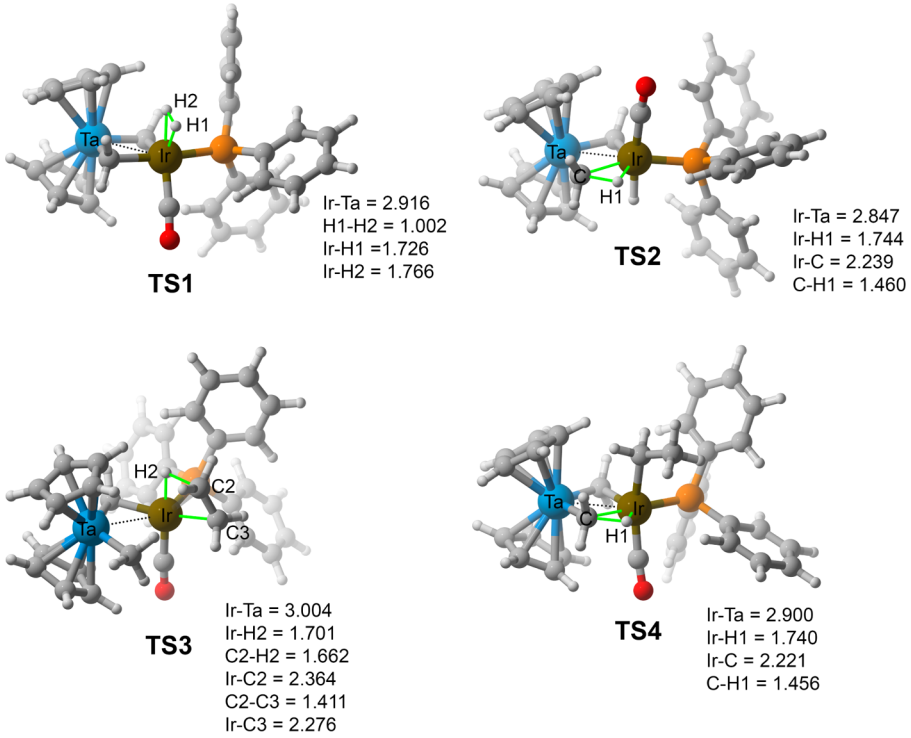

Figure 3. Key transition-state structures for catalytic cycle III. Bond distances reported in angstroms.

hydride to liberate ethane and regenerate **1a** with $\Delta H^{\ddagger}$ = 3.9 kcal/mol relative to **1a**.

On the enthalpy landscape for catalytic cycle III, the Ir−H intermediate **J** is exothermic by 20.1 kcal/mol, and the enthalpy span from **J** up to transition state **TS5** suggests that this catalytic step controls the rate of turnover;[29] however, inspection of the free energy landscape reveals that the migratory insertion transition state **TS3** is turnover-limiting in the complete catalytic cycle III.

We also explored the possibility that during cycle III, PPh_3 dissociates from each intermediate. Our calculations suggest that this is unlikely. For example, the H_2 oxidative addition activation enthalpy increases to >20 kcal/mol when PPh_3 dissociates. In addition, reductive elimination of the hydride and μ-CH_2 groups requires a >35 kcal/mol activation enthalpy without PPh_3 coordination. Unfortunately, experiments by Bergman and co-workers are inconclusive about PPh_3 dissociation for catalyst **1a** since the addition of excess PPh_3 to catalyst **1a** resulted in the formation of a new and unidentified species.[22]

The original report by Bergman and co-workers favored the full catalytic cycle III for catalyst **1a** because: (1) Reaction of **1a** with dihydrogen resulted in the spectroscopically characterized equilibrium with the dihydride $[Cp_2Ta(CH_2)_2Ir(H)_2(CO)(PPh_3)]$ complex **F**; (2) deuterium exchange studies showed that under an excess of D_2, all four methylene positions become deuterated; and (3) the rate of hydrogenation is first order in **1a**, dihydrogen, and alkene.

Our calculations show that the reaction pathway for catalytic cycle III is, indeed, lower in enthalpy than the reaction pathways for catalytic cycles I and II. However, there is also the possibility that once the Ir-Et intermediate **I** is formed, there is then a short circuit catalytic loop to generate ethane and regenerate the Ir−H intermediate **G** without returning to the original heterobimetallic complex **1a**. The shortened catalytic cycle is depicted by the red arrows in Scheme 2. This catalytic cycle loops among intermediates **G**, **H**, and **I**.

The enthalpy landscape for the short circuit catalytic loop is shown at the top of Figure 4. Similarly to the full catalytic cycle III, this short circuit loop begins with ethylene coordination to Ir−H **G** and migratory insertion through **TS3** to give intermediate **I**. The H_2 oxidative addition transition state **TS6** (Figures 4, 5) converts **I** into the cis dihydride **K** that is exothermic by 23.6 kcal/mol. The $\Delta H^{\ddagger}$ via **TS6** for H_2 oxidative addition is 4.4 kcal/mol relative to intermediate **I**. This activation enthalpy is 7.2 kcal/mol lower in enthalpy than **TS4**. The free energy landscape is shown at the bottom of Figure 4. The $\Delta G^{\ddagger}$ via **TS6** for H_2 oxidative addition is 13.7 kcal/mol relative to intermediate **I**. This activation free energy is 1.3 kcal/mol higher in free energy than **TS4**. This suggests that that full catalytic cycle III and the short circuit cycle are competitive, and it is likely that significant amounts of alkene hydrogenation proceed through the short circuit loop. We favor the short circuit loop resulting in the majority of alkene hydrogenation because the comparison of **TS6** and **TS4** is better evaluated on the enthalpy surface since **TS4** is an intramolecular transitions state and **TS6** is an intermolecular transition state and likely overestimates the translational entropy penalty. This short catalytic loop is finished and reforms Ir−H **G** by reductive elimination through **TS7** with $\Delta H^{\ddagger}$ = −9.7 kcal/mol, relative to **1a** (and intermediate **G**).

Ir−P catalyst. As a comparison with catalyst **1a**, Figure 6 shows the enthalpy surface for catalytic cycle III with the Ir−P catalyst **1b**. All intermediates related to catalyst **1b** are named with lower case letters. The most critical feature of this enthalpy landscape in relationship to Figure 2 is that the reductive elimination of the cis dihydride intermediate **f** via **TS2b** has a significantly larger barrier than **TS2**. The $\Delta H^{\ddagger}$ for **TS2b** is 28.2 kcal/mol. This is ∼18 kcal/mol larger than **TS2**. Also different,

DOI: 10.1021/cs501884j
ACS Catal. 2015, 5, 1840−1849

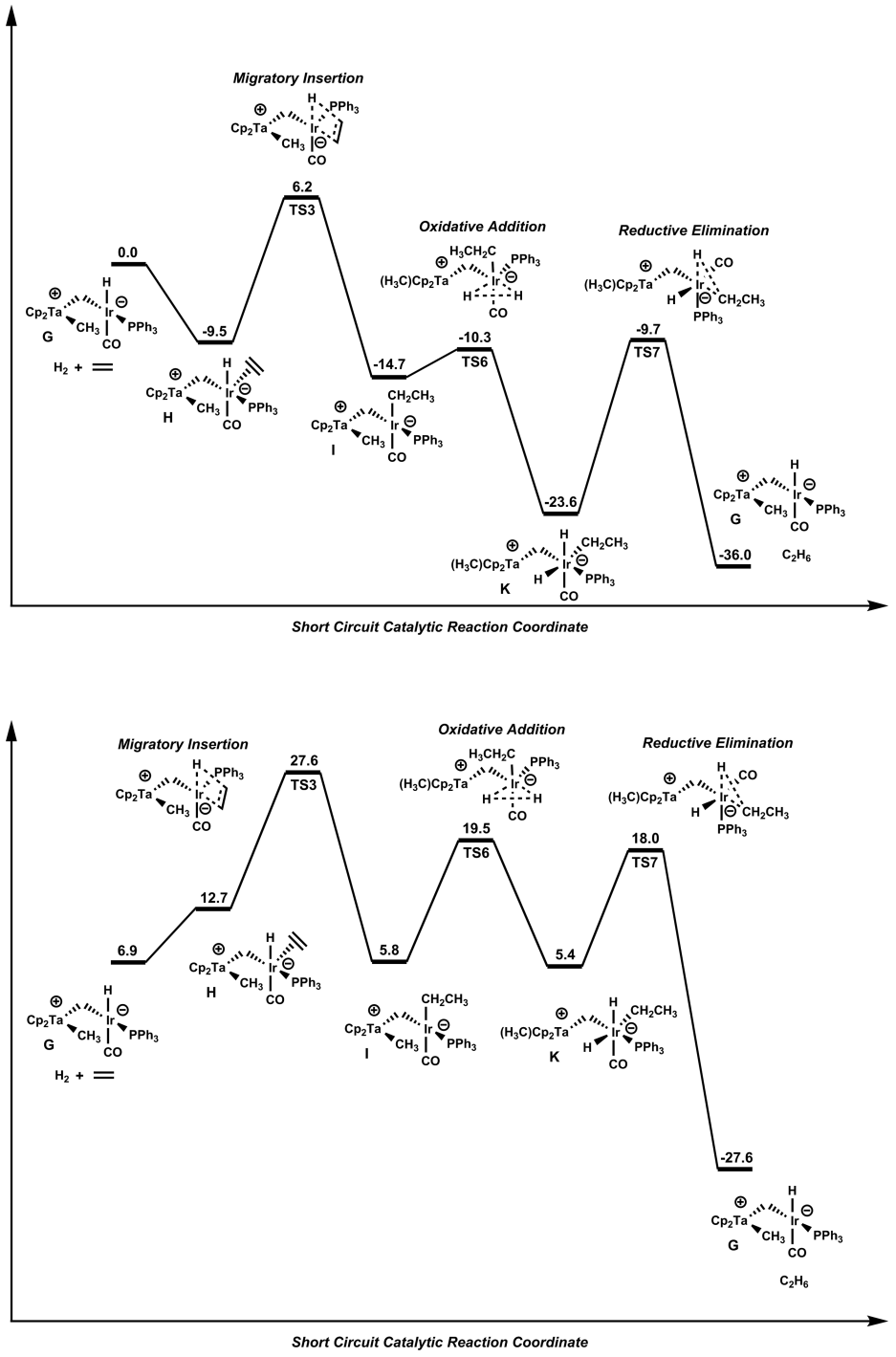

Figure 4. M06 enthalpy (top) and free energy (bottom) landscapes for the short circuit catalytic loop. (kcal/mol).

intermediates **g**, **h**, and **i** are ∼10 kcal/mol more exothermic than the corresponding intermediates in Figure 2.

The large activation barrier for **TS2b** compared with **TS2** is unexpected, given the structural similarity of complexes **1a** and **1b** and results in a different catalytic cycle presented later that is lower in enthalpy. This high enthalpy transition state **TS2b** also accounts for why there is experimentally no deuterium incorporation into the μ-CH_2 bridge. The origin of the high enthalpy reductive elimination transition state can be attributed to two effects and is not correlated with the corresponding reaction step thermodynamics: (1) the relative electron density at the metal center that enables Ir^{III} to Ir^{I} reduction; (2) the relative stability of the μ-CH_2 anion ligand that is involved in reductive elimination.

Although relative electron densities on the Ir metal center undoubtedly have an effect on the relative reductive elimination barriers, we suggest that the more impactful effect is that the cationic Cp_2Ta group, compared to the cationic PPh_2 group, induces greater transition state stabilization of developing partial carbon anion character on the methylene group during reductive elimination. This is supported by an ∼20 kcal/mol lower proton affinity for $[Cp_2Ta(CH_3)_2]^+ \rightarrow [Cp_2Ta(CH_3)(CH_2)] + H^+$ compared to $[P(CH_3)_4]^+ \rightarrow [P(CH_3)3(CH_2)] +$

DOI: 10.1021/cs501884j
ACS Catal. 2015, 5, 1840−1849

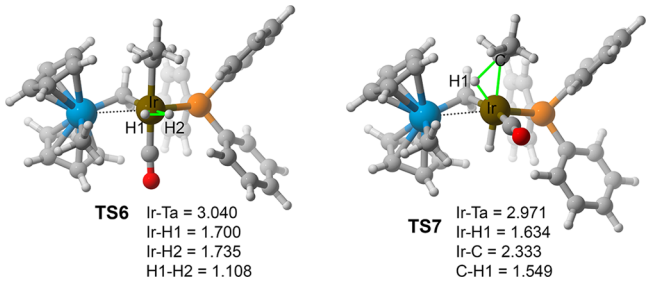

Figure 5. **TS6** and **TS7** from the short circuit catalytic cycle. Bond distances reported in angstroms.

H^+. Similarly, $[Cl_2Ta(CH_3)_2]^+$ has an ∼15 kcal/mol lower proton affinity than $[Cl_2P(CH_3)_2]^+$.

The most plausible catalytic cycle identified by calculations for complex **1b** is shown in Figure 7. Analogous to cycle III, this catalytic cycle begins with H_2 oxidative addition via **TS1b** to give the cis dihydride **f**. This pathway is lower in enthalpy than PPh_3 dissociation prior to **TS1b**. At intermediate **f**, the mechanism diverges from catalytic cycle III. Rather than reductive elimination of the Ir−H and μ-CH_2 groups due to the prohibitively high activation barrier, there is an energetically feasible PPh_3 dissociation pathway (ΔH = 18.8 kcal/mol relative to **1b**) that forms the 5-coordinate intermediate **b**. This phosphine dissociation pathway is consistent with experiments by Bergman and co-workers, who showed that excess PPh_3 inhibits alkene hydrogenation with complex **1b**. Additionally, the μ-CH_2 groups in catalyst **1b** do not undergo deuterium exchange with D_2. This mechanism is not operative for complex **1a** because intermediate **B** (see Figure 1) is significantly higher in energy than transition state **TS2** (see Figure 2).

Ligand rearrangement and ethylene coordination to complex **b** results in the 6-coordinate trans dihydride complex **c**, which is ∼4 kcal/mol lower in enthalpy than cis dihydride geometries. The trans dihydride geometry also provides the lowest energy pathway for ethylene to insert into the Ir−H bond via **TS6b** with $\Delta H^{\ddagger}$ = 12.7 kcal/mol. The resulting Ir−Et intermediate **d** then easily undergoes reductive elimination via transition state **TS7b** ($\Delta H^{\ddagger}$ = 6.7 kcal/mol) to give ethane and regenerate **1b** with PPh_3 recoordination. The Ir−P catalytic cycle (cycle IV) corresponding to the enthalpy landscape presented in Figure 7 is shown in Scheme 3. The bottom of Figure 7 also reports the free energy landscape of the proposed mechanism for catalyst **1b**. On this free energy landscape, the barriers for H_2 oxidative addition and Ir−H migratory insertion are very similar, and at this level of computational treatment, it is unclear which of these two reaction steps is predicted to control the rate of turnover.

We have also examined the possibility that catalytic cycle IV is short circuited. For example, it is possible that the Ir-CO intermediate **l** undergoes H_2 oxidative addition faster than recoordination of PPh_3 (Scheme 3, orange arrow). We have discounted this possibility because the $\Delta H^{\ddagger}$ for oxidative addition of H_2 without PPh_3 is 7.0 kcal/mol larger than that for **TS1b**. A second short circuit cycle is also possible in which the Ir-Et intermediate **d** reacts with H_2 to generate ethane and the Ir cis dihydride intermediate **b**. This catalytic cycle bypasses all 3-coordinate Ir intermediates as well as complex **1b**. Unlike for catalytic cycle III, the only pathway possible for the conversion of Ir-Et **d** into the cis dihydride **b** is via concerted H_2 1,2 addition across the Ir-Et bond. This pathway requires $\Delta H^{\ddagger}$ = 14.0 kcal/mol relative to Ir-Et **d**. This activation enthalpy is significantly larger than the $\Delta H^{\ddagger}$ = 6.4 kcal/mol relative to Ir-Et **d** for reductive elimination of the hydride and ethyl groups to generate **l**.

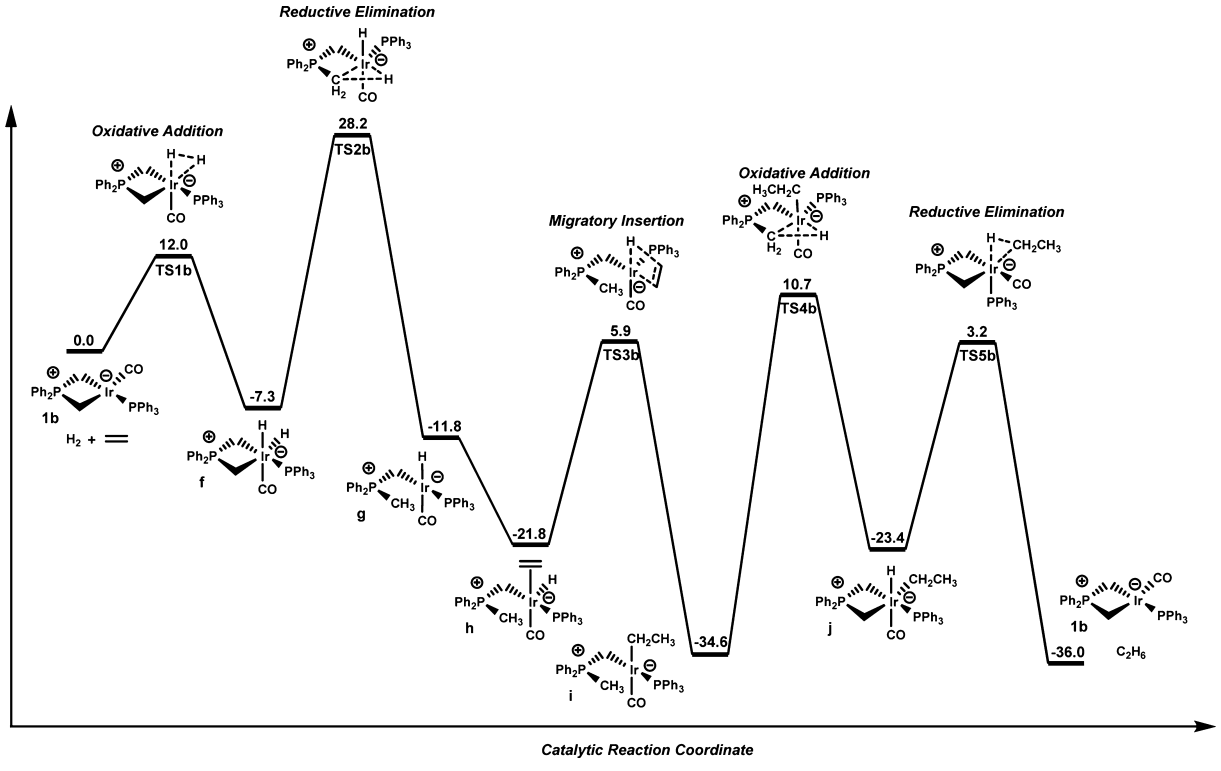

Figure 6. M06 enthalpy landscape for catalytic cycle III with catalyst **1b**. (kcal/mol).

DOI: 10.1021/cs501884j
ACS Catal. 2015, 5, 1840−1849

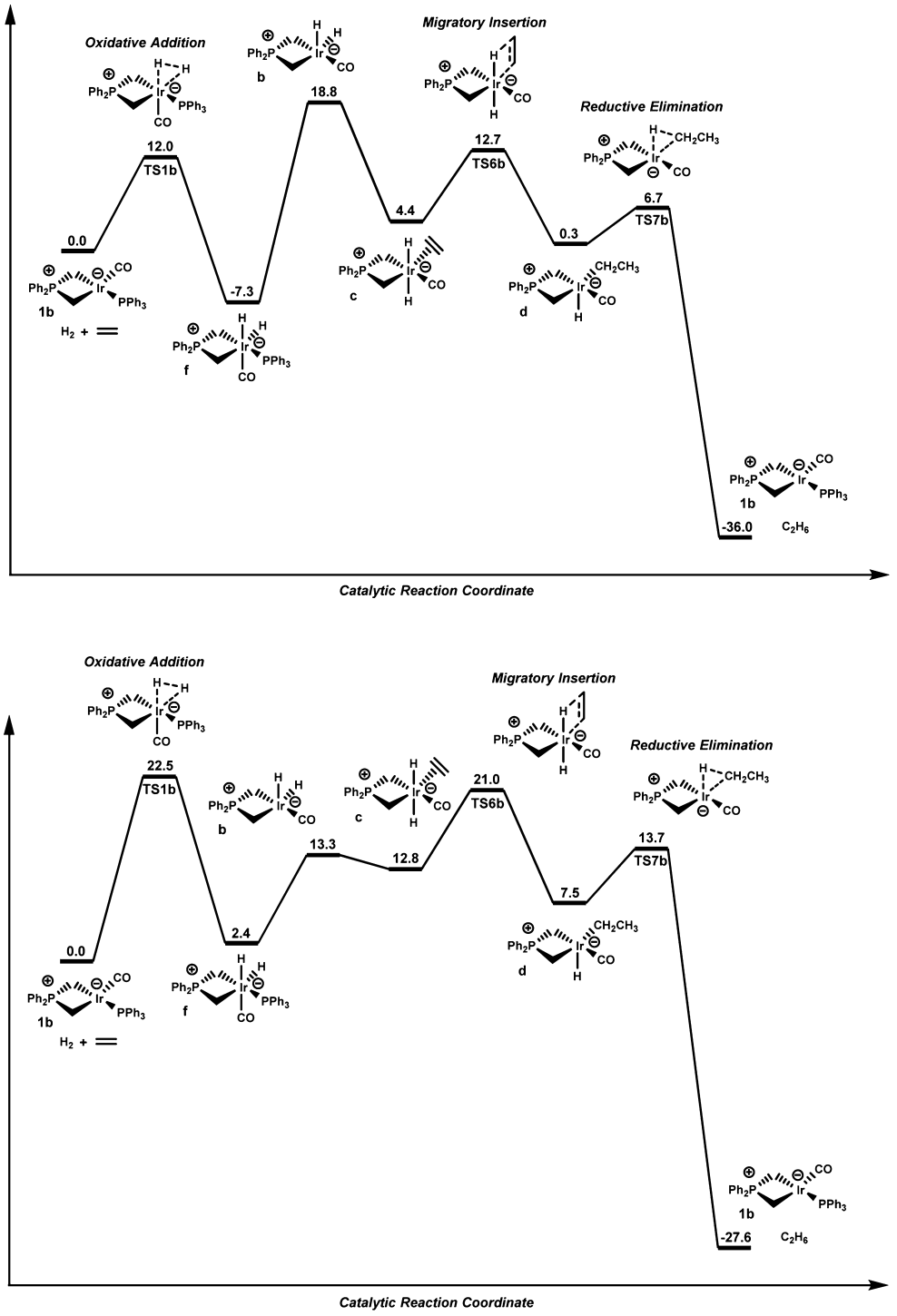

Figure 7. M06 enthalpy (top) and free energy (bottom) landscapes for proposed mechanism of catalyst **1b**. (kcal/mol).

CONCLUSIONS

DFT modeling of alkene hydrogenation by the $Cp_2Ta(CH_2)_2Ir(CO)(PPh_3)$ **1a** complex and the $Ph_2P(CH_2)_2Ir(CO)(PPh_3)$ **1b** complex revealed several important features of heterobimetallic catalysis versus transition metal/main group catalysis: (1) Calculations indicate that the Ir−Ta and the Ir−P catalysts operate by different mechanisms. (2) The Ir−Ta complex undergoes precursor transformation to an active heterobimetallic Ir−H species that likely catalyzes multiple turnovers of alkene hydrogenation before reforming the original heterobimetallic Ir−Ta complex. The Ir−H short circuit catalytic cycle involves ethylene coordination, migratory insertion, H_2 oxidative addition, and reductive elimination of ethane. (3) The key step in the precursor transformation is the reductive elimination of hydride and μ-CH_2 groups. (4) This precursor transformation does not occur for the Ir−P catalyst because the reductive elimination activation barrier is significantly higher in energy. (5) The Ir−Ta catalyst is proposed to undergo much faster reductive elimination of the hydride and μ-CH_2 groups compared with the Ir−P catalyst as a result of greater stabilization of α carbon anion character in the transition state by the cationic Cp_2Ta group. This

DOI: 10.1021/cs501884j
ACS Catal. 2015, 5, 1840−1849

Scheme 3. Alkene Hydrogenation Catalytic Cycles for Complex 1b

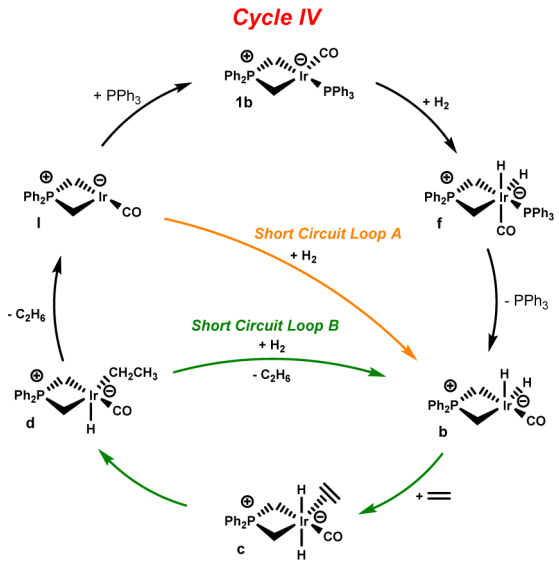

conclusion is supported by the lower proton affinity for $[Cp_2Ta(CH_3)_2]^+$ versus $[P(CH_3)_4]^+$. (6) In the Ir−P mechanism, the $Ph_2P(CH_2)_2$ group remains as a spectator ligand throughout the active catalytic cycle. (7) The Ir−P catalytic cycle involves H_2 oxidative addition, phosphine ligand dissociation, ethylene migratory insertion, and reductive elimination of ethane.

Overall, this study showcases the possibility of utilizing a nontraditional ligand scaffold that involves a direct transition metal−transition metal interaction to control the operation of a catalytic cycle and achieve a mechanism that is different from a monometallic transition metal catalyst. The recent resurgence of synthesis and use of heterobimetallic catalysts provides new direction for catalyst design that will potentially impact inorganic transformations as well as enable new reactivity and selectivity in organic synthesis. Further insights into the operation of heterobimetallic catalysts will also provide a link between homogeneous single-site metal catalysis and heterogeneous catalysis.

■ ASSOCIATED CONTENT

Supporting Information

The following file is available free of charge on the ACS Publications website at DOI: 10.1021/cs501884j.

Energies and *xyz* coordinates (PDF)

■ AUTHOR INFORMATION

Corresponding Author

*E-mail: dhe@chem.byu.edu.

Notes

The authors declare no competing financial interest.

■ ACKNOWLEDGMENTS

D.H.E. thanks Brigham Young University (BYU) and the Fulton Supercomputing Lab (FSL). Sam Roberts thanks the BYU Department of Chemistry and Biochemistry for an undergraduate research award.

■ REFERENCES

(1) (a) Bullock, R. M.; Casey, C. P. *Acc. Chem. Res.* **1987**, *20*, 167. (b) Stephan, D. W. *Coord. Chem. Rev.* **1989**, *95*, 41. (c) Wheatley, N.; Kalck, P. *Chem. Rev.* **1999**, *99*, 3379. (d) Thomas, C. M. *Comments Inorg. Chem.* **2011**, *32*, 14.

(2) For bimetallic complexes, see: (a) Sinfelt, J. H. *Acc. Chem. Res.* **1977**, *10*, 15. (b) Sinfelt, J. H. *Bimetallic Catalysts: Discoveries, Concepts and Applications*; John Wiley and Sons: New York, 1983.

(3) For early examples of heterobimetallic complexes and their reactions, see: (a) Ferguson, G. S.; Wolczanski, P. T. *Organometallics* **1985**, *4*, 1601. (b) Ferguson, G. S.; Woczanski, P. T.; Párkányi, L.; Zonnevylle, M. C. *Organometallics* **1988**, *7*, 1967. (c) Casey, C. P. *J. Organomet. Chem.* **1990**, *400*, 205. (d) Pinkes, J. R.; Steffey, B. D.; Vites, J. C.; Cutler, A. R. *Organometallics* **1994**, *13*, 21. (e) Baranger, A. M.; Bergman, R. G. *J. Am. Chem. Soc.* **1994**, *116*, 3822. (f) Butts, M. D.; Bergman, R. G. *Organometallics* **1994**, *13*, 1899. (g) Hanna, T. A.; Baranger, A. M.; Bergman, R. G. *J. Am. Chem. Soc.* **1995**, *117*, 11363. (h) Baranger, A. M.; Hanna, T. A.; Bergman, R. G. *J. Am. Chem. Soc.* **1995**, *117*, 10041. (i) Aubart, M. A.; Bergman, R. G. *J. Am. Chem. Soc.* **1996**, *118*, 1793.

(4) (a) Lin, T.-P.; Wade, C. R.; Pérez, L. M.; Gabbaï, F. P. *Angew. Chem., Int. Ed.* **2010**, *49*, 6357. (b) Jayarathne, U.; Mazzacano, T. J.; Bagherzadeh, S.; Mankad, N. P. *Organometallics* **2013**, *32*, 3986. (c) Ma, M.; Sidiropoulos, A.; Ralte, L.; Stasch, A.; Jones, C. *Chem. Commun.* **2013**, *49*, 48.

(5) For an example of transition metal/main group complexes, see: (a) Betley, T. A.; Peters, J. C. *J. Am. Chem. Soc.* **2003**, *125*, 10782. (b) Thomas, J. C.; Peters, J. C. *Inorg. Chem.* **2003**, *42*, 5055. (c) Thomas, C. M.; Peters, J. C. *Organometallics* **2005**, *24*, 5858. (d) Pang, K.; Quan, S. M.; Parkin, G. *Chem. Commun.* **2006**, 5015. (e) Figueroa, J. S.; Meinick, J. G.; Parkin, G. *Inorg. Chem.* **2006**, *45*, 7056. (f) Landry, V. K.; Melnick, J. G.; Buccella, D.; Pang, K.; Ulichny, J. C.; Parkin, G. *Inorg. Chem.* **2006**, *45*, 2588. (g) Sircoglou, M.; Bontemps, S.; Bouhadir, G.; Saffon, N.; Miqueu, K.; Gu, W.; Mercy, M.; Chen, C.-H.; Foxman, B. M.; Maron, L.; Ozerov, O. V.; Bourissou, D. *J. Am. Chem. Soc.* **2008**, *130*, 16729. (h) Bontemps, S.; Sircoglou, M.; Bouhadir, G.; Puschmann, H.; Howard, J. A. K.; Dyer, P. W.; Miqueu, K.; Bourissou, D. *Chem.—Eur. J.* **2008**, *14*, 731. (i) For an example of H_2 activation see: Lin, T.-P.; Peters, J. C. *J. Am. Chem. Soc.* **2013**, *135*, 15310. (j) Fong, H.; Moret, M.-E.; Lee, Y.; Peters, J. C. *Organometallics* **2013**, *32*, 3053. (k) Harman, W. H.; Lin, T.-P.; Peters, J. C. *Angew. Chem., Int. Ed.* **2014**, *53*, 1081.

(6) Slaughter, L. M.; Wolczanski, P. T. *Chem. Commun.* **1997**, 2109.

(7) Uyeda, C.; Peters, J. C. *Chem. Sci.* **2013**, *4*, 157.

(8) (a) Greenwood, B. P.; Forman, S. I.; Rowe, G. T.; Chen, C.-H.; Foxman, B. M.; Tomas, C. M. *Organometallics* **2009**, *48*, 6251. (b) Greenwood, B. P.; Towe, G. T.; Chen, C.-H.; Foxman, B. M.; Tomas, C. M. *J. Am. Chem. Soc.* **2010**, *132*, 44. (c) Setty, V. N.; Zhou, W.; Foxman, B. M.; Thomas, C. M. *Inorg. Chem.* **2011**, *50*, 4647. (d) Kuppuswamy, S.; Bezpalko, M. W.; T. M; Turnbull, M. M.; Foxman, B. M.; Thomas, C. M. *Inorg. Chem.* **2012**, *51*, 8225. (e) Rudd, P. A.; Liu, S.; Planas, N.; Bill, E.; Gagliardi, L.; Lu, C. C. *Angew. Chem., Int. Ed.* **2013**, *52*, 4449. (f) Tereniak, S. J.; Carlson, R. K.; Clouston, L. J.; Young, V. G., Jr.; Bill, E.; Maurice, R.; Chen, Y.-S.; Kim, H.-J.; Gagliardi, L.; Lu, C. C. *J. Am. Chem. Soc.* **2014**, *136*, 1842. (g) Karunananda, M. K.; Vazquez, F. X.; Alp, E. E.; Bi, W.; Chattopadhyay, S.; Shibata, T.; Mankad, N. P. *Dalton Trans.* **2014**, Advance Article, 10.1039/C4DT01841A.

(9) (a) Cooper, B. G.; Fafard, C. M.; Foxman, B. M.; Thomas, C. M. *Organometallics* **2010**, *29*, 5179. (b) Curley, J. J.; Bergman, R. G.; Tilley, T. D. *Dalton Trans.* **2012**, *41*, 192.

(10) For a theoretical description of heterobimetallic bond polarity, see: Jansen, G.; Schubart, M.; Findeis, B.; Gade, L. H.; Scowen, I. J.; McPartlin, M. *J. Am. Chem. Soc.* **1998**, *120*, 7239.

(11) (a) Krogman, J. P.; Bezpalko, M. W.; Foxman, B. M.; Thomas, C. M. *Inorg. Chem.* **2013**, *52*, 3022. (b) Jayarathne, U.; Parmelee, S. R.; Mankad, N. P. *Inorg. Chem.* **2014**, *53*, 7730.

(12) Thomas, C. M.; Napoline, J. W.; Rowe, G. T.; Foxman, B. M. *Chem. Commun.* **2010**, *46*, 5790.

DOI: 10.1021/cs501884j
ACS Catal. 2015, 5, 1840−1849

(13) (a) Memmler, H.; Kauper, U.; Gade, L. H.; Scowen, I. J.; McPartlin, M. *Chem. Commun.* **1996**, 1751. (b) Gade, L. H.; Memmler, H.; Kauper, U.; Schneider, A.; Fabre, S.; Bezougli, I.; Lutz, M.; Galka, C.; Scowen, I. J.; McPartlin, M. *Chem.—Eur. J.* **2000**, *6*, 692.
(14) Uyeda, C.; Peters, J. C. *J. Am. Chem. Soc.* **2013**, *135*, 12023.
(15) Zhou, W.; Saper, N. I.; Krogman, J. P.; Foxman, B. M.; Thomas, C. M. *Dalton Trans.* **2014**, *43*, 1984−1989.
(16) Tsutsumi, H.; Sunada, Y.; Shiota, Y.; Yoshizawa, K.; Nagashima, H. *Organometallics* **2009**, *28*, 1988.
(17) (a) Hostetler, M. J.; Butts, M. D.; Bergman, R. G. *Organometallics* **1993**, *12*, 65. (b) Zhou, W.; Marquard, S. L.; Bezpalko, M. W.; Foxman, B. M.; Thomas, C. M. *Organometallics* **2013**, *32*, 1766.
(18) (a) Gelmini, L.; Stephan, D. W. *Organometallics* **1988**, *7*, 849. (b) Choukroun, R.; Dahan, F.; Gervais, D.; Rifaï, C. *Organometallics* **1990**, *9*, 1982. (c) Dickson, R. S.; De Simone, T.; Campi, E. M.; Jackson, W. R. *Inorg. Chim. Acta* **1994**, *220*, 187.
(19) Lindenberg, F.; Shribman, T.; Sieler, J.; Hey-Hawkins, E.; Eisen, M. *J. Organomet. Chem.* **1996**, *515*, 19.
(20) (a) Ceccon, A.; Gambaro, A.; Santi, S.; Valle, G.; Venzo, A. *J. Chem. Soc., Chem. Commun.* **1989**, 51. (b) Bonifaci, C.; Ceccon, A.; Gambaro, A.; Ganis, P.; Mantovani, L.; Santi, S.; Venzo, A. *J. Organomet. Chem.* **1994**, *475*, 267.
(21) Mazzacano, T. J.; Mankad, N. P. *J. Am. Chem. Soc.* **2013**, *135*, 17258.
(22) (a) Hostetler, M. J.; Bergman, R. G. *J. Am. Chem. Soc.* **1990**, *112*, 8621. (b) Hostetler, M. J.; Butts, M. D.; Bergman, R. G. *Inorg. Chim. Acta* **1992**, *198−200*, 377. (c) Hostetler, M. J.; Butts, M. D.; Bergman, R. G. *J. Am. Chem. Soc.* **1993**, *115*, 2743. (d) Butts, M. D.; Bergman, R. G. *Organometallics* **1994**, *13*, 2668.
(23) For synthesis of a Pd-Ta complex, see: Butts, M. D.; Bergman, R. G. *Organometallics* **1994**, *13*, 1899.
(24) For recent examples of Ir-catalyzed hydrogenation mechanisms of π bonds, see: (a) Margalef, J.; Caldentey, X.; Karlsson, E. A.; Coll, M.; Mazuela, J.; Pàmies, O.; Diéguez, M.; Pericàs, M. A. *Chem.—Eur. J.* **2014**, *20*, 12201. (b) Dobereiner, G. E.; Nova, A.; Schley, N. D.; Hazari, N.; Miller, S. J.; Eisenstein, O.; Crabtree, R. H. *J. Am. Chem. Soc.* **2011**, *133*, 7547. (c) Mazuela, J.; Norrby, P.-O.; Andersson, P. G.; Pàmies, O.; Diéguez, M. *J. Am. Chem. Soc.* **2011**, *133*, 13634. (d) Church, T. L.; Rasmussen, T.; Andersson, P. G. *Organometallics* **2010**, *29*, 6769. (e) Brandt, P.; Hedberg, C.; Andersson, P. G. *Chem.—Eur. J.* **2003**, *9*, 339.
(25) Frisch, M. J.; Trucks, G. W.; Schlegel, H. B.; Scuseria, G. E.; Robb, M. A.; Cheeseman, J. R.; Scalmani, G.; Barone, V.; Mennucci, B.; Petersson, G. A.; Nakatsuji, H.; Caricato, M.; Li, X.; Hratchian, H. P.; Izmaylov, A. F.; Bloino, J.; Zheng, G.; Sonnenberg, J. L.; Hada, M.; Ehara, M.; Toyota, K.; Fukuda, R.; Hasegawa, J.; Ishida, M.; Nakajima, T.; Honda, Y.; Kitao, O.; Nakai, H.; Vreven, T.; Montgomery, J. A., Jr.; Peralta, J. E.; Ogliaro, F.; Bearpark, M.; Heyd, J. J.; Brothers, E.; Kudin, K. N.; Staroverov, V. N.; Kobayashi, R.; Normand, J.; Raghavachari, K.; Rendell, A.; Burant, J. C.; Iyengar, S. S.; Tomasi, J.; Cossi, M.; Rega, N.; Millam, M. J.; Klene, M.; Knox, J. E.; Cross, J. B.; Bakken, V.; Adamo, C.; Jaramillo, J.; Gomperts, R.; Stratmann, R. E.; Yazyev, O.; Austin, A. J.; Cammi, R.; Pomelli, C.; Ochterski, J. W.; Martin, R. L.; Morokuma, K.; Zakrzewski, V. G.; Voth, G. A.; Salvador, P.; Dannenberg, J. J.; Dapprich, S.; Daniels, A. D.; Farkas, Ö.; Foresman, J. B.; Ortiz, J. V.; Cioslowski, J.; Fox, D. J. *Gaussian 09, Revision B.01*; Gaussian, Inc.: Wallingford, CT, 2009.
(26) (a) Zhao, Y.; Truhlar, D. G. *Theor. Chem. Acc.* **2008**, *120*, 215. (b) Zhao, Y.; Truhlar, D. G. *Acc. Chem. Res.* **2008**, *41*, 157.
(27) (a) Ehlers, A. W.; Bohme, M.; Dapprich, S.; Gobbi, A.; Hollwarth, A.; Jonas, V.; Kohler, K. F.; Stegmann, R.; Veldkamp, A.; Frenking, G. *Chem. Phys. Lett.* **1993**, *208*, 111. (b) Roy, L. E.; Hay, P. J.; Martin, R. L. *J. Chem. Theory Comput.* **2008**, *4*, 1029.
(28) Marenich, A. V.; Cramer, C. J.; Truhlar, D. G. *J. Phys. Chem. B* **2009**, *113*, 6378.
(29) Kozuch, S.; Shaik, S. *Acc. Chem. Res.* **2011**, *44*, 101.

DOI: 10.1021/cs501884j
ACS Catal. 2015, 5, 1840−1849